Metal Stamped Antenna-in-Package for Millimeter-wave Large-scale Phased-array Applications Using Multiphysics Analysis

Junho Park, Wonbin Hong*
[1] Pohang University of Science and Technology (POSTECH): Department of Electrical Engineering, Pohang, South Korea,
* *whong@postech.ac.kr*

***Abstract*—This paper presents a metal stamped antenna-in-package concept for enhanced cooling in millimeter-wave (mmWave) phased array systems. To verify the proposed AiP concept, the proof-of-concept (POC) model is designed and fabricated using standard PCB and metal stamping process. The fabricated POC model achieves -10 dB impedance bandwidth of 0.7 GHz with a center frequency of 28.5 GHz. Good agreement is achieved between the measured and simulated radiation patterns with the measured peak gain of 14.01 dBi. The effect of the fabrication error on EM properties is discussed to explain the difference between the simulated and measured results of the gain. The two-dimensional array is demonstrated to verify the feasibility for a practical application of mmWave Massive MIMO systems with main beam scanning range of ± 30° in both elevation and azimuth planes. Computational fluid dynamics simulation confirms that the proposed metal stamp AiP reduces the maximum surface temperature of the package by more than 11 ºC.**

***Index Terms*—Phased-array, Antenna-in-Package, 5G, millimeter-wave, heat dissipation.**

I. INTRODUCTION

Amid the deployment of fast-emerging millimeter-wave (mmWave) communication systems, phased array transceiver and advanced antenna packaging technologies have been extensively studied and presented [1]-[3]. In mmWave phased array system, each antenna element requires a variety of active components including phased-shifter, low-noise amplifier, power amplifier, and Tx/Rx switch for high radiated power and wide beam-scanning range [4]. However, the low power amplifier efficiency [5] (typically less than 25 %) poses a significant challenge for thermal management for phased-array module packaging aspects [6]. In addition, small cell systems with massive number of RF channels can generate a very large amount of heat from the high dissipated power of the entire system. Therefore, thermal management should be thoroughly addressed during the design process to guarantee reliability of phased array systems that operate under various environmental conditions.

Considering that the heat generated from the conventional phased array configuration is concentrated in the center of the array [7], the excess heat should be transferred to a heat exchanger or to ambient air. Active cooling systems have received much attention due to their effective heat removal capability [8], [9]. The microchannel heat sink with a ladder-shaped inlet header is proposed and embedded in the highly integrated phased-array antenna module for cooling the internal heat and reducing temperature non-uniformity [8]. Forced air cooling and forced liquid cooling are investigated for the Ka-band active phased array [9]. However, active

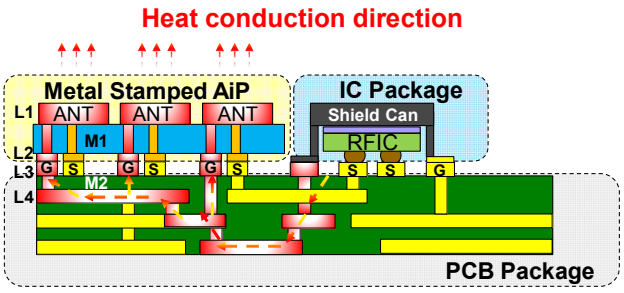

(a)

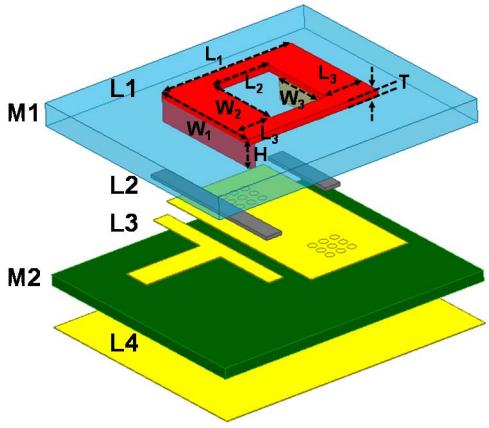

(b)

Fig. 1. (a) The conceptual diagram of the proposed metal stamped AiP. (b) The detailed view of the antenna element.

TABLE I
ANTENNA PARAMETERS

Parameter	Value (mm)	Parameter	Value (mm)
W_1	3	L_1	3.5
W_2	2	L_2	1.5
W_3	1.5	L_3	1
H	0.55	T	0.15

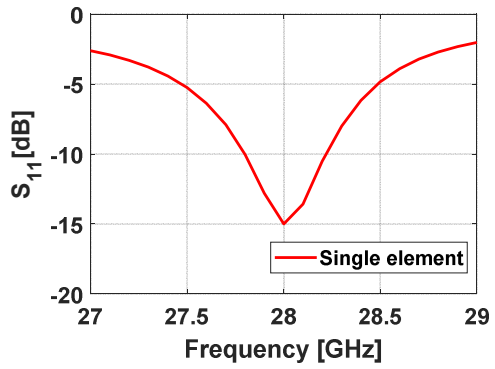

Fig. 2. Simulated $|S_{11}|$ of the metal stamped antenna element.

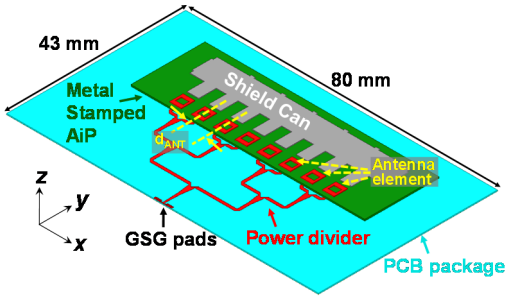

Fig. 3. Configuration of the metal stamped AiP POC

cooling systems are not suitable for high-volume applications due to energy efficiency issues, cost issues, and increased complexity of the entire system.

Passive thermal management can be more cost-effective and energy-efficient solution. The dissipated power is efficiently removed by a heat spreader connecting the transistor to the antenna [10]. The 3-D fractal heatsink antenna is proposed to alleviate the thermal resistance in [11]. However, a relatively bulky heatsink antenna configuration is inappropriate to be applied for compact mmWave phased arrays with flexible beam-scanning capability.

In this paper, we propose a compact stamped antenna-in-package (AiP) structure that can be directly integrated with the transceiver module and expanded in the form of modular configuration. The proposed AiP not only maximizes the heat removal capability in the passive level but also features good radiation performances. Section II introduces the basic concept of the proposed packaging methods and fabricates the proof-of-concept (POC) model by using stamping process, which is completely compatible with present-day mass production process. Section III analyzes the electromagnetic and thermomechanical characteristics of the proposed AiP. The two-dimensional array based on the proposed AiP topology is designed and demonstrated in Section IV. Section V concludes this paper.

II. Design Process

A. Metal Stamped Antenna-in-Package Overview

Fig. 1 (a) presents the conceptual diagram of the proposed AiP concept, which can be classified into several parts named

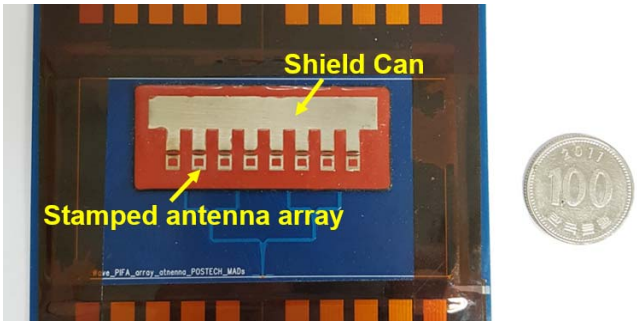

Fig. 4. Photograph of the fabricated metal stamped AiP POC.

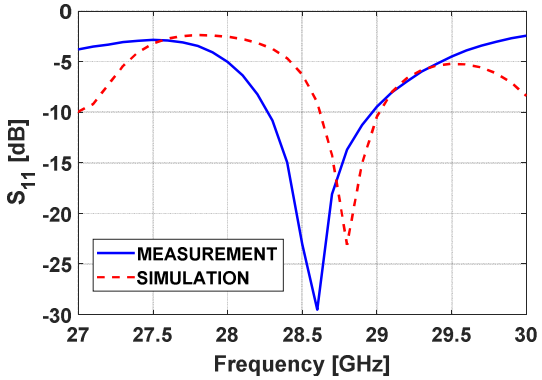

Fig. 5. Simulated and measured $|S_{11}|$ of the metal stamped AiP POC.

the metal stamped AiP, the IC package, and the PCB package. The metal stamped AiP can be directly connected to the RFIC mounted on the PCB using the vertical transition structure and soldering process. The metal stamped AiP dually functions as a phased-array antenna module and a heat spreader, which transfers heat from the IC to ambient air.

In the metal stamped AiP, the planar inverted-F antenna (PIFA) antenna is selected as a basic topology for the following reasons: 1) Since the PIFA antenna is a planar structure and includes a large opening surface, it can easily be manufactured using the stamping process. 2) The PIFA antenna requires a short pin, which can be connected to the thermal pads or vias, efficiently transfer the conducted heat to ambient air. 3) A large opening surface and a wide feeding structure of the PIFA antenna maximize the contact area of the antenna, increasing heat removal capability. The detailed antenna structure is shown in Fig. 1 (b) and the dimensions are summarized in Table 1. As illustrated in Fig. 1 (b), the radiating elements (L1 to L2) molded from the stamping process are deposited on the dielectric substrate (M1) with ε_r = 3.55 and tan σ = 0.001 using thermal bonding. Ground and signal pads (L3 to L4) are printed on the dielectric substrate of Rogers RT 5880 dielectric substrate (M2) with ε_r = 2.2, tan σ = 0.0009, and thickness of 0.254 mm. The optimized model is simulated using the 3-D EM solver, Ansys HFSS and features 420 MHz (27.8 to 28.22 GHz) impedance bandwidth, as illustrated in Fig. 2.

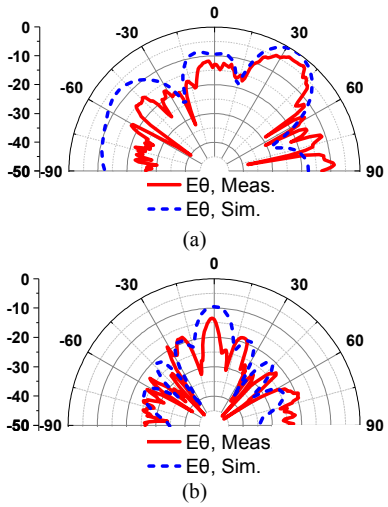

Fig. 6. Measured and simulated normalized radiation patterns for the metal stamped AiP POC. (a) E_θ in the *yz* plane. (b) E_θ in the *xz* plane.

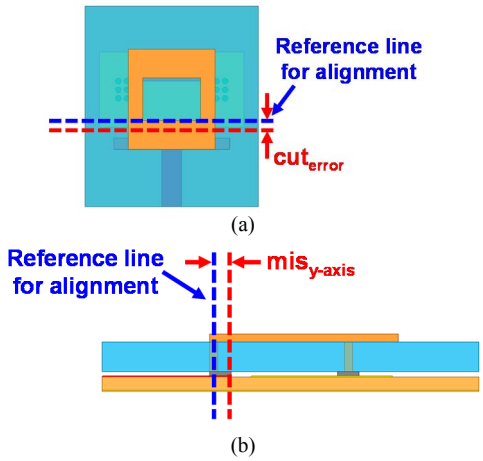

Fig. 7. Geometry of the metal stamped AiP: (a) The top-view after stamping. (b) The side-view after soldering.

B. *Proof-of-Concept Model*

The POC model is designed and fabricated using the previously designed antenna element. The proposed AiP POC model consists of the PCB package and the metal stamped AiP with 8 antenna elements for emulating antenna array properties, as illustrated in Fig. 3. The overall size of the POC model is 80 mm × 43 mm. The ground-signal-ground (GSG) pad for antenna evaluation is configured on the top side of the PCB package. Each antenna element of the metal stamped AiP is arranged at a distance (d_{ANT}) of 5.6 mm which is 0.53 λ_0 at 28.5 GHz. The metal stamped AiP is adhesively mounted on the PCB package using solder paste. The dummy shield can structure is used to align the two packages during the soldering process. The signal pad of each antenna is connected to the 1:8 power divider.

III. Results and Discussion

Fig. 4 illustrates a photograph of the fabricated POC model after soldering process. The S-parameters are measured by using Keysight PNA-X. The 3-D EM simulation is performed to extract the reflection coefficients and the antenna properties using Ansys HFSS.

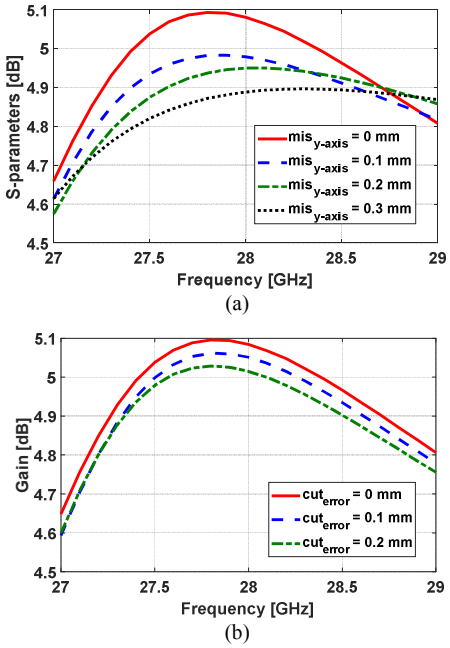

Fig. 8. Simulated realized gain of the proposed metal stamped antenna element (a) as a function of $mis_{y\text{-}axis}$. (b) as a function of cut_{error}.

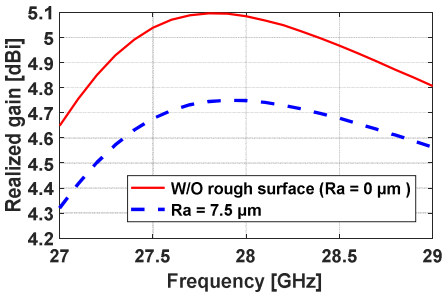

Fig. 9. Simulated realized gain of the proposed metal stamped antenna element including the surface roughness model.

A. *Antenna Package Characterization*

The measured and simulated reflection coefficients (Fig. 5) of the metal stamped AiP POC feature – 10 dB impedance bandwidths of 700 MHz and 400 MHz respectively. It can be seen that the measured operating frequency is slightly lower than the simulated one. These discrepancy is dominantly attributed to the deviation of the electrical characteristics of the dielectric substrate and fabrication errors in the metal stamping process.

The far-field radiation patterns (Fig. 6) of the POC model are measured in a probe-based anechoic chamber described in [12]. The measured far-field radiation patterns of the POC model correlate well with 3-D EM simulation results. The E-plane radiation pattern (Fig. 6 (a)) shows that the main lobe is tilted by 30° due to the position of the PIFA antenna on the fixed ground plane. However, the direction of the main lobe

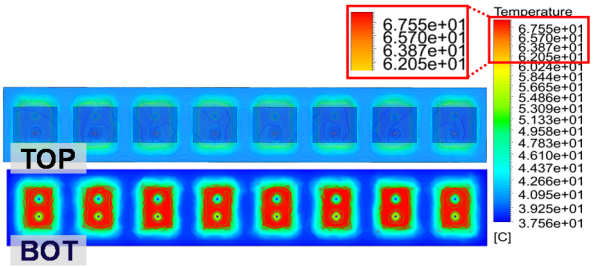

(a)

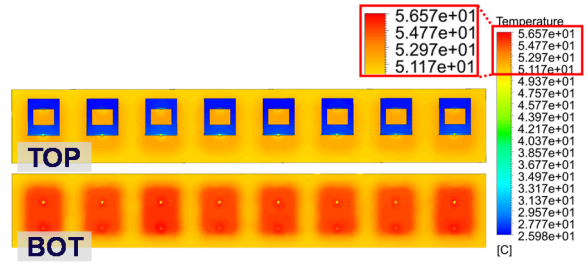

(b)

Fig. 10. Comparison of simulated temperature distribution (a) The reference patch antenna array. (b) The proposed metal stamped AiP.

can be easily adjusted by configuring two-dimensional phased array, which will be demonstrated in Section IV. It is confirmed in Fig. 6 (b) that the beam is synthesized by combining the 8-element linearly polarized antennas. The simulated and measured results feature a peak realized gain of 16.47 and 14.09 dBi respectively. The gain deviation between the measured and simulated results is further investigated in the next sub-section.

B. Electrical Stability of the Fabrication Process

The antenna gain and the input impedance of the proposed AiP are significantly influenced by the misalignment between the PCB package and the metal stamped AiP during the soldering process, the machining error during the metal stamping process, and the rough surface of conductors. First, the effect of the misalignment is investigated. While $mis_{y\text{-}axis}$ is set to be 0 mm in an ideal condition, the misalignment (Fig. 7 (a)) exists in the fabrication process. It is confirmed in Fig. 8 (a) that the gain of the antenna deteriorates when $mis_{y\text{-}axis}$ gets larger. Second, the machining error during the stamping process is also one of the factors affecting the antenna properties. The parameter cut_{error} is depicted in Fig. 7 (b). The effect of the machining error (cut_{error}) is studied in Fig. 8 (b). The simulation results demonstrate that the gain of the antenna deteriorates when cut_{error} gets larger.

Third, the effect of the rough surface on the antenna properties is simulated with the use of the average value of the rough surface (Ra). The range of Ra after the heat-treated stainless steel finish is typically between 3.5 and 7.5 μm [13]. The Huray model [14] is used to simulate the effect of the rough surface on the antenna properties. Fig. 9 demonstrates losses due to surface roughness by a conventional stainless metal surface finish. Therefore, the unavoidable loss caused by the fabrication error, conductive joints, and conductor

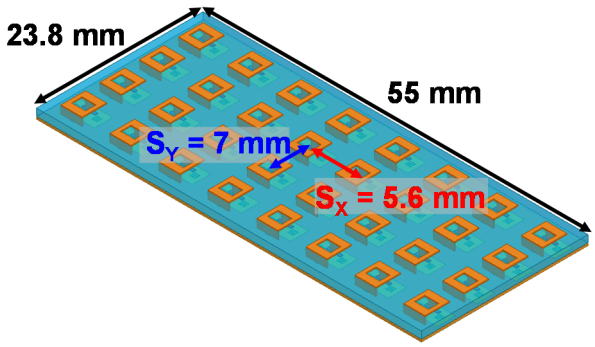

Fig. 11. 3-D View of the 4 × 8 metal stamped AiP structure.

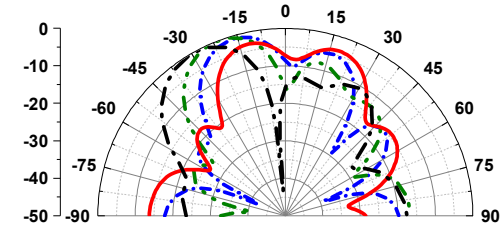

(a)

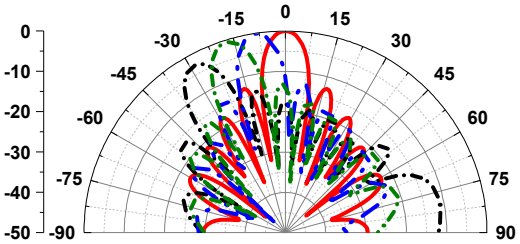

(b)

Fig. 12. Simulated beam steering radiation patterns of the 4 × 8 metal stamped AiP structure. (a) E-plane (φ). (b) H-plane (θ).

surface roughness should be included in the design stage using the efficient numerical simulation methodology for accurate prediction of the antenna properties.

C. Thermal-Mechanical Analysis

To verify the heat removal capability of the proposed metal stamped AiP, an 8-element patch antenna array (Fig. 10 (a)) is designed using identical design conditions of the POC model for objective evaluation. The optimized width and length of the radiating patch are 4.1 mm and 3.3 mm, respectively. For the computational fluid dynamics (CFD) simulation, a virtual RFIC is positioned at the bottom of the PCB package of the POC model and each RF channel of the RFIC is electrically connected to the feedline of the antenna element through vertical interconnection. The temperature distribution (Fig. 10 (b)) of the two structures are simulated under the condition of the ambient temperature of 25 °C using Ansys Fluent. The reference model features the maximum temperature of 67.55 °C, while the proposed structure features relatively lower 56.57 °C. In addition, it can be seen that the heat is effectively transferred from the RFIC on the PCB package to the top of the metal stamped package.

TABLE II
COMPARISON WITH HEAT SINK ANTENNAS

	[10]	[11]	This work
Topology	Patch	Patch	4 × 8 PIFA
Center frequency (GHz)	2	1.43	28.5
Boresight Gain (dBi)	5	7.15	13.5 (array gain)
Scanning angle (°)	N/A	N/A	± 30° [a]
Element Volume (λ_g^3)	0.66 × 0.66 × 0.36	0.38 × 0.38 × 0.3	0.62 × 0.53 × 0.1

[a] In both elevation and azimuth plane

IV. 32-ELEMENT METAL STAMPED PHASED-ARRAY AIP

Although one-dimensional array is designed and analyzed in this paper, the proposed antenna topology can easily be extended to two-dimensional array structure using vertically interconnect structures (vias) for large-scale phased array applications. The 4 × 8 metal stamped AiP is exemplified in Fig. 11.

The inter-element spacing, S_X = 5.6 mm in the horizontal direction (0.53 λ_0 at 28.5 GHz) and S_Y = 7 mm in the vertical direction (0.66 λ_0 at 28.5 GHz), are chosen using the numerically analyzed results to minimize the sidelobe level (SLL). The radiation patterns of the 4 × 8 metal stamped AiP are illustrated in Fig. 12. The 4 × 8 metal stamped AiP achieves the boresight gain of 13.5 dBi at φ = 0° and a scanning angle of ± 30° with a maximum SLL less than -10 dB in azimuth plane at 28.5 GHz.

Table II compares this work with the latest relevant works. It is noted that the proposed metal stamped AiP is a firstly reported mmWave phased-array consisting of heat sink antenna elements with wide beam-scanning ranges.

V. CONCLUSION

This paper demonstrates a first-of-its-kind metal stamped AiP solution based on a stamping process, which can contribute to the cost-effective phased array module for mmWave massive MIMO applications. The proposed AiP features good radiation performance with an efficient heat removal capability. The two-dimensional array is implemented in the form of modular design, significantly improving the beam-scanning range in both elevation and azimuth directions. It is expected that the proposed design methodology can be widely utilized for future mmWave transceiver modules based on the electromagnetic-thermomechanical co-design process.

ACKNOWLEDGMENT

This work was partially supported by Samsung Electronics and the Institute of Information & Communications Technology Promotion (IITP) grant funded by the Korean government (MIST) (No. 2018-0-00733), and Next Generation Engineering Researcher Program of National Research Foundation of Korea (NRF) funded by the Ministry of Science, ICT (grant number: 2019H1D8A2106519). The authors thank ANSYS Korea for their generous support. In addition, the authors are also grateful to Young-Hoon Min and Eunbong Han of Samsung Electronics Research Division, Seoul, South Korea for their insightful comments, as well as the manufacturing of the AiP module.

REFERENCES

[1] W. Roh et al., "Millimeter-wave beamforming as an enabling technology for 5G cellular communications: theoretical feasibility and prototype results," IEEE Commun. Mag., vol. 52, no. 2, pp. 106-113, Feb. 2014.

[2] K. Kibaroglu, M. Sayginer and G. M. Rebeiz, "A low-cost scalable 32-element 28-Ghz phased array transceiver for 5G communication links based on a 2 × 2 beamformer flip-chip unit cell," J. Solid-State Circuits, vol. 53, no. 5, pp. 1260-1274, May 2018.

[3] J. Park, H. Seong, Y. N. Whang and W. Hong, "Energy efficient 5G phased-arrays incorporating vertically-polarized endfire planar folded slot antenna for mmwave mobile terminals," IEEE Trans. on Antennas Propag., in press

[4] W. Hong, K. Baek, Y. Lee, Y. Kim and S. Ko, "Study and prototyping of practically large-scale mmwave antenna systems for 5G cellular devices," IEEE Commun. Mag., vol. 52, no. 9, pp. 63-69, Sep. 2014.

[5] J. D. Dunworth et al., "A 28GHz Bulk-CMOS dual-polarization phased-array transceiver with 24 channels for 5G user and basestation equipment," in Proc. of IEEE Int. Solid-State Circuits Conf. (ISSCC) Dig. Tech. Papers, San Francisco, CA, USA, Feb. 2018, pp. 70-72.

[6] Y. Aslan, J. Puskely, J. H. J. Janssen, M. Geurts, A. Roederer and A. Yarovoy, "Thermal-aware synthesis of 5G base station antenna arrays: an overview and a sparsity-based approach," IEEE Access, vol. 6, pp. 58868-58882, Oct. 2018.

[7] E. McCune, "Energy efficiency maxima for wireless communications: 5G, IoT, and massive MIMO," in Proc. of 2017 IEEE Custom Integrated Circuits Conference (CICC), TX, USA, 2017, pp. 1-8.

[8] J. Zhou, L. Yin, L. Kang, M. Wang and J. Huang, "Joint design and experimental tests of highly integrated phased-array antenna with microchannel heat sinks," IEEE Antennas and Wireless Propag. Lett, in press

[9] B. J. Döring, "Cooling system for a Ka band transmit antenna array," German Aerospace Center (DLR), Köln, Germany, Tech. Rep. IB554-06/02, Dec. 2005.

[10] A. Alnukari, P. Guillemet, Y. Scudeller and S. Toutain, "Active heatsink antenna for radio-frequency transmitter," IEEE Trans. Adv. Packag., vol. 33, pp. 139-146, Feb. 2010.

[11] J. J. Casanova, J. A. Taylor and J. Lin, "Design of a 3-D fractal heatsink antenna," IEEE Antennas and Wireless Propag. Lett., vol. 9, pp. 1061-1064, Nov. 2010.

[12] J. Park, S. Y. Lee, J. Kim, D. Park, W. Choi, W. Hong, "An optically invisible antenna-on-display (AoD) concept for millimeter-wave 5G cellular devices," IEEE Trans. on Antennas Propag., vol. 67, no. 5, pp. 2942-2952, May. 2019.

[13] "Roughness measurements of stainless steel surfaces," 2014 [Online]. Available: http://www.worldstainless.org/Files/issf/non-image-files/PDF/Euro_Inox/RoughnessMeasurement_EN.pdf

[14] S. Hall and H. Heck, Advance Signal Integrity for High-Speed Digital Designs. Hoboken, NJ, USA: Wiley, 2009.